16. J. Ahn and J. W. Rabalais, *Surf. Sci.* **388**, 121 (1997).
17. P. Guenard, G. Renaud, A. Barbier, M. Gautier-Soyer, *Surf. Rev. Lett.* **5**, 321 (1997).
18. T. Hiemstra, H. Yong, W. H. Van Riemsdijk, *Langmuir* **15**, 5942 (1999).
19. D. A. Sverjensky and N. Sahai, *Geochim. Cosmochim. Acta* **60**, 3773 (1996).
20. CTR diffraction is done by measuring diffuse scattering between Bragg points as a function of perpendicular momentum transfer into the substrate. This diffuse CTR scattering aligns normal to the surface and arises from breaking bulk translation symmetry due to the presence of an interface or surface. Surface relaxations and reconstructions and the presence of overlayer atoms modulate the signal along these rods of scattering. For an introduction to the technique see I. K. Robinson and D. J. Tweet, *Rep. Prog. Phys.* **55**, 599 (1992); G. Renaud, *Surf. Sci. Rep.* **32**, 1 (1998); P. Fenter *et al.*, *Geochim. Cosmochim. Acta* 64, 1221 (2000).
21. The crystal wafer obtained from Union Carbide Crystal Products (Washougal, WA) was 0.5 mm thick and 50 mm in diameter, with a rms roughness of about 1 Å, based on x-ray reflectivity measurements, and a miscut of <0.3°, based on orientation measurements during the CTR work. The wafer was prepared with a mild acid etch (10 mM HNO_3) followed by multiple rinses with MilliQ water and heating to 350°C in air. After cooling to room temperature, it was immediately subjected to an extensive wash with MilliQ water and blown dry with an argon jet. Similarly prepared wafers have been studied by our group using photoemission and atomic force microscope, as reported in (*5*).
22. In previous work (*5–9*), the hydration reaction was found to be dissociative, leading to surface hydroxyl groups.
23. The structure factor is determined by taking the square root of the background-subtracted integrated intensity corrected for active area, polarization, step size, and Lorentz factor [I. K. Robinson, in *Handbook on Synchrotron Radiation*, vol. 3, G. Brown and D. E. Moncton, Eds. (Elsevier, Amsterdam, 1991), pp. 221–266].
24. The structure of α-Al_2O_3 (space group $R\bar{3}c$) consists of a distorted hexagonal close-packed layer sequence of oxygens, with aluminum occupying two-thirds of the octahedral holes. The oxygen stacking sequence runs along the *c* axis, and a unit cell consists of six oxygen layers, giving six formula units per unit cell. The Al atoms are staggered along the *c* direction about a plane centered between the oxygen layers, and the oxygen atoms are slightly displaced in-plane from their ideal positions. The staggered positions of the Al atoms lead to two sets of Al-O bond lengths. The Al that is displaced in the positive direction along the *c* axis has three short Al-O bonds (1.86 Å) to the oxygen layer above and three long Al-O bonds (1.97 Å) to the oxygen layer below. The reverse is the case for the Al that is displaced in the negative direction along the *c* axis. The cell parameters used in this work (a = 4.757 Å, c = 12.988 Å) are from [A. Kirfel and K. Eichhorn, *Acta Crystallogr. A* **46**, 271 (1990)], with bulk isotropic Debye-Waller factors from [N. Ishizawa, T. Miyata, I. Minato, F. Marumo, S. Iwai, *Acta Crystallogr. B* **36**, 228 (1980)].
25. For each of the three chemical terminations, there are six crystallographically distinct terminations depending on where the unit cell is cut. Because they are chemically equivalent, the six terminations must be equally probable, and therefore our model consisted of equal weighting of these terminations, with the same fit parameters (displacements, Debye-Waller factors, and occupancies) used for each.
26. B.-D. Yan, S. L. Meilink, G. W. Warren, P. Wynblatt, *IEEE Trans. Components Hybrids Manufact. Technol.* **CHMT-10**, 247 (1987).
27. The (00L) rod is sensitive only to ordering in the direction perpendicular to the surface and is unaffected by the degree of lateral ordering. The dominant free parameter in the overlayer model is the *z* position of the layer. The Debye-Waller factor acts as a measure of layer disorder even though the actual structure is likely to be more complex. A more accurate description of the layer involves a continuous electron density distribution normal to the surface; however, extensive specular reflectivity data are required to uniquely determine such a distribution.
28. Seven independent displacement parameters, four Debye-Waller factors, and four layer occupancies were used in the least-squares fitting procedure. Only the parameters for the top five layers were allowed to vary in the final fit. Varying additional parameters for deeper layers did not significantly improve the χ^2 value; therefore, they were held at their bulk positions in the final fit. The α-Al_2O_3 (0001) surface has p3 symmetry, with Al atoms positioned at the centers of the threefold axis and the oxygens arranged about the threefold axis. To maintain symmetry in our surface model, we displaced the Al atoms only along the *z* direction and we constrained the oxygen atoms to maintain trigonal symmetry.
29. There exists some debate (*15–17*) about the termination as well as the layer spacing for the clean UHV surface. Guenard *et al.* (*17*) find (Fig. 2A) an Al-terminated surface with a 51% contraction for the first layer, whereas Ahn and Rabalais (*16*) find a 63% contraction. Toofan and Watson (*15*) find a mixed Al/O termination with expansion of the top layer. Surface preparation variation resulting in, for example, residual OH could account for these differences.
30. M. Gautier *et al.*, *J. Am. Ceram. Soc.* **77**, 323 (1994).
31. V. Coustet and J. Jupille, *Surf. Sci.* **307-309**, 1161 (1994).
32. J. G. Chen, J. E. Crowell, J. T. Yates, *J. Chem. Phys.* **84**, 5906 (1986).
33. I. D. Brown and D. Altermatt, *Acta Crystallogr. B* **41**, 244 (1985).
34. L. Pauling, *The Nature of the Chemical Bond* (Cornell University Press, Ithaca, NY, ed. 3, 1960), pp. 547–559.
35. J. R. Bargar, S. N. Towle, G. E. Brown Jr., G. A. Parks, *J. Colloid Interface Sci.* **185**, 473 (1997).
36. K. Wefers and C. Misra, *Oxides and Hydroxides of Aluminum, Alcoa Technical Paper No. 19, Revised* (Alcoa Laboratories, Alcoa Center, PA, 1987).
37. Differences in stability were used by Liu *et al.* (*5*) to predict the threshold pressure for hydroxylation of the α-Al_2O_3 (0001) surface to be 2.8 torr and 6.3 torr based on gibbsite and bayerite free energies, respectively. This result agrees well with the measured threshold pressure of about 1 torr for hydroxylation of the α-Al_2O_3 (0001) surface, as determined by O 1s photoemission spectroscopy (*5*). It has also been observed that Al hydroxides (gibbsite and bayerite) are formed on water-immersed α-Al_2O_3 [D. H. Lee and R. A. Condrate Sr., *Mater. Lett.* **23**, 241 (1995)] and γ-Al_2O_3 [C. Dyer, P. J. Hendra, W. Forsling, M. Ranheimer, *Spectrochim. Acta* **49A**, 691 (1993); E. Laiti, P. Persson, L-O. Öhman, *Langmuir* **14**, 825 (1998)] powder surfaces.
38. S. N. Towle, J. R. Bargar, G. E. Brown Jr., G. A. Parks, *J. Colloid Interface Sci.* **217**, 312 (1999).
39. J. P. Fitts, T. P. Trainor, D. Grolimund, G. E. Brown Jr., G. A. Parks, unpublished data.
40. J. A. Kelber, C. Niu, K. Shepherd, D. R. Jennison, A. Bogicevic, *Surf. Sci.* **446**, 76 (2000).
41. Supported by Department of Energy (DOE) grant DE-FG03-93ER14347-A007 (Stanford University), DOE grant DE-FGO2-94ER14466, National Science Foundation grant EAR-9906456, and the W. M. Keck foundation (GeoSoilEnviroCARS, University of Chicago). Use of the Advanced Photon Source was supported by the DOE, Basic Energy Sciences, Office of Energy Research, under contract W-31-109-ENG-38. We thank J. Fitts, D. Grolimund, F. Sopron, and N. Lazarz for their assistance with the measurements and J. V. Smith for constructive comments on the manuscript.

21 December 1999; accepted 22 March 2000

Rapid Flooding of the Sunda Shelf: A Late-Glacial Sea-Level Record

Till Hanebuth,* Karl Stattegger, Pieter M. Grootes

The increase in sea level from the last glacial maximum has been derived from a siliciclastic system on the tectonically stable Sunda Shelf in Southeast Asia. The time from 21 to 14 thousand calendar years before the present has been poorly covered in other records. The record generally confirms sea-level reconstructions from coral reefs. The rise of sea level during meltwater pulse 1A was as much as 16 meters within 300 years (14.6 to 14.3 thousand years ago).

Sea-level curves of the last deglaciation have been constructed from coral reefs by means of U/Th or radiocarbon dating of corals [e.g., Barbados (*1, 2*), Tahiti (*3, 4*), New Guinea (*5, 6*)]. The Barbados record contains only a few clustered data points between larger intervals without data for the early phase of the late-glacial sea-level rise; the Tahiti record starts at 13.8 thousand years ago (ka) (all ages are in calendar kiloyears before present) (*7*) above a late Pleistocene reef unit; and the New Guinea record starts at 13.1 ka and is situated in an area with strong tectonic uplift. There is a prominent hiatus in most records corresponding to the meltwater pulse (MWP) 1A around 14 ka (*2*). Catastrophic sea-level rise for that time is interpreted in the Caribbean-Atlantic region from an abrupt deepening of the coral assemblages (*8*). From these and other records, two alternative models of the eustatic late- to postglacial sea-level rise have been proposed (*9*): (i) a continuous model in which sea level rose steadily with varying transgression rates and (ii) an episodic model in which sea level rose in steps with several pauses or even erosion in between.

Here we present a record of the late-glacial transgression on the Sunda Shelf, the largest shelf area outside the polar regions, covering an area of 1.8×10^6 km^2 between the Indonesian archipelago and Vietnam. During the last glacial

Institute of Geosciences, University of Kiel, Olshausenstrasse 40, 24 118 Kiel, Germany.

*To whom correspondence should be addressed. E-mail: th@gpi.uni-kiel.de

maximum (LGM), the Sunda Shelf was widely subaerially exposed. The adjacent South China Sea was strongly reduced in size, forming a semi-enclosed marginal sea. This exposed a large low-gradient coastal plain on the Sundaland craton. The Singapore platform in its central part was tectonically stable during the Pliocene and Pleistocene, and the modern Malayan Peninsula and Borneo and Sumatra islands formed highlands to the south (*10*). Several river systems, originating here, drained the coastal lowlands during the LGM and the first phase of late-glacial flooding (*11*); the largest paleoriver system is known as the North Sunda River or Molengraaff River and flowed to the northeast (*12*).

More than 50 sediment cores along two transects were collected during cruise 115 of R/V *Sonne*: One transect was oriented northeast to southwest and extended 600 km from the upper continental slope to the middle shelf in the area of the former North Sunda River. The second transect ran east to west off the modern Mekong Delta for 200 km (*13*). The sedimentary records were used to determine position relative to sea level at the time of deposition by analysis of the depositional environment. We identified mangrove swamps, mud flats, and coarser grained siliciclastic deposits from the base of the transgressive system (*14*) that formed in a microtidal environment with a tidal range of less than 2 m (*15*). Analysis of terrestrial organic material (pollen, wood fragments, in situ mangrove roots, peaty layers) provided additional information on terrigenous sources of sediments.

We obtained accelerator mass spectrometry (AMS) radiocarbon dates of terrestrial organic material along several cores to follow the coastline migration in time and space (*16*). Because sediments can consist of a complex mixture of recent terrestrial and marine biological products and older reworked organic and inorganic carbon-containing terrestrial and marine material, clearly identifiable material is required for meaningful dates. We dated mangrove roots, larger wood fragments (centimeter sized), and coarse-grained peaty detritus in tidal flat deposits as direct sea-level indicators (*17*). In addition, we dated plant material from the landward delta plain as well as from the seaward bay lagoon and delta front environment and benthic foraminifera (*Rotalia* sp.) from the oldest purely marine part. Because transport and reworking of organic material may cause a bias in the determination of sea-level ages, we tried to estimate the effect on age determinations of mixing different terrigenous organic materials. Residues of the acid-alkali-acid extraction of peaty layers and organic macrofossils such as larger wood fragments and in situ root remnants yielded the youngest and most reliable ages. The differences in age between macro- and microplant remnants in sediments containing <1% C_{org} are up to 1500 years, and the larger biases are toward younger ages, which may be explained by increased reworking and admixture of older detritus as sea level rises. The dates from alkali-extracted organic material (humic acids) were generally somewhat older than the macrofossils and peat but younger than the organic-poor residues. An additional indicator for recognition of fresh organic material and a measure of rapid primary deposition is the ash content, which depends on microbial decay, reworking, and early diagenetic processes (*18*).

On the proximal part of the Sunda Shelf transect, the late-glacial transgression could be directly followed between a water depth of 70 and 126 m. Pedogenesis on the late Pleistocene land surface indicates a low sea-level stillstand in the LGM at 22 ka. This surface is overlaid by transgressive coastal sediments. These are partly cut by incised channels detected from shallow seismic surveying, which belong to the ultimate phase of the North Sunda River system before marine flooding. Rapid lateral and vertical facies changes, extreme sedimentation pulses, and/or hiatuses of several thousand years characterize the record between 21.0 and 13.4 ka in 37 cores (*19*). Cores from the Vietnamese part of the Sunda Shelf in similar depositional environments yielded ages between 13.0 and 11.0 Ka corresponding to depths between 56 and 48 m. Fully marine sands then cover the transgressive sediments after a hiatus. Ages from *Rotalia* sp. from this cover layer vary widely from 12.4 to 4.1 ka and indicate that these shelf sediments were reworked and mixed up to recent times (*14*, *20*).

We present the first half of the late to postglacial sea-level curve from the Sunda Shelf (Fig. 1) as a probability band, taking into account the uncertainties (1σ) of relevant data in both age and position relative to present sea level (*7*, *21*). The curve can be divided into four segments.

Between 21.0 and 19.0 ka, the terminal phase of the LGM, sea level rose slowly from -116 to -114 m below modern sea surface at a rate of 0.10 m per 100 years (1σ = 0.14 m per 100 years). Compared with the 2-m tidal range, this sea-level rise is statistically not significant and it is therefore poorly defined (segment 1).

Between 19.0 and 14.6 ka, sea level rose moderately from -114 to -96 m at a rate of 0.41 m per 100 years ($1\sigma = \pm0.08$ m per 100 years) (segment 2).

Between 14.6 and 14.3 ka, sea level rose from -96 to -80 m at an accelerated rate of 5.33 m per 100 years. The large 1σ range and the impossibility of quoting the 1σ probability areas, which lead to a very asymmetric distribution of possible calibrated ages, results from ^{14}C calibration over the Oldest Dryas/Bølling ^{14}C plateau. The possible rate estimated from probability distributions of calibrated ages ranges from 2.8 to 16 m per 100 years. A high value of 16 m is unrealistic because of the local sediment accumulation rate and the ability of mangroves to settle (segment 3).

Between 14.3 and 13.1 ka, sea level rose more gradually from -80 to -64 m at a rate of 1.33 m per 100 years ($1\sigma = \pm0.33$ m per 100 years) (segment 4).

The younger sea level rise up to 11 ka is represented by only two data points from the Vietnam Shelf that indicate an average rise of 8 m in 700 years.

Segments 2 and 3 of our curve with control points covering the whole time range fill substantial time intervals without data points in the coral reef sea-level records. For segment 2, data from 16.6 to 15.4 ka are derived from three cores characterized by a moderate and continuous acceleration in sea-level rise filling a gap of 3 ka in the Barbados curve (*1*). Segment 3 is characterized by a rapid rise in sea level of 16 m.

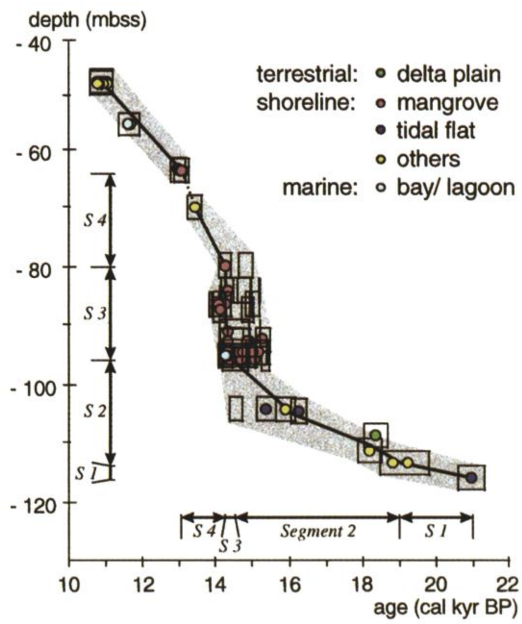

Fig. 1. Sea-level curve for the Sunda Shelf derived from shoreline facies. Colored points: most probable ages. Rectangles: vertical, maximum tidal extension; horizontal, 1σ probability. Gray band, range of 1σ and tidal influence; black line, most probable position of sea-level curve. ^{14}C plateaus can cause multiple age points and error bars (rectangles) within the 1σ probability containing no age point (*20*). For explanation of segments, see text. mbss = meters below sea surface.

This rapid rise is resolved by 17 dates on plant fragments (14) and in situ preserved mangrove root remnants (3) from five cores. A ^{14}C plateau extending from 15.3 to 14.4 ka is probably caused by large changes in oceanic circulation related to the strong MWP 1A (*7*). This ^{14}C plateau causes ambiguities in the conversion of ^{14}C ages to calibrated ages. Two age values in the lower half of the sudden rise are slightly younger than the end of the plateau, indicating that the youngest of the multiple age values of the plateau ages fit best to the curve. The start of segment 3 is defined as the average of the two calibration intercepts at 14.7 and 14.4 ka in core 5981; the intercept at 15.1 is impossible considering the age of the Oldest Dryas/Bølling transition at 14.65 ka in the GISP2 ice core (*21*). Similarly, at the end of this segment in 80-m water depth at 14.3 ka, the statistical 2σ probability allows a young age of maximal 14.08 ka in core 5609.

The Sunda Shelf sea-level curve is compared with other published curves plotted on the U/Th time scale or on the ^{14}C time scale newly calibrated using INTCAL98/CALIB 4.0 (*7*) (Fig. 2). For segments 2 and 3, we observe a remarkable agreement between the U/Th-dated Barbados sea-level curve and the ^{14}C-dated Sunda Shelf sea-level curve. The recalibrated ^{14}C ages of the Barbados curve not used for sea-level reconstruction, however, are 300 to 500 years younger. This indicates that the calibration based on U/Th data gives good results for ^{14}C of terrigenous material but that discrepancies may occur for marine calibrations for a variety of reasons (*22*). The shape of MWP 1A calculated from the Sunda Shelf data is similar to MWP 1A calculated from Barbados. This is all the more remarkable, considering the larger uncertainty envelopes of both curves. It confirms that there is no evidence of a true sea-level jump but that the rise took place faster than has been suggested (*1, 2, 8*). The depth precision of the present sea-level record is determined by the tidal range of 2 m on the Sunda Shelf; this is narrower than the one resulting from the coral habitat zonation of 6 m in coral reefs.

The phase of accelerated sea-level rise was attributed to MWP 1A, which started at 14.7 ka and ended at 14.1 ka in correspondence to the first cold reversal of the Bølling-Allerød observed in the GISP2 core (*3, 4, 23*). MWP 1A was previously described as a large sea-level jump before 13.8 ka (*2*), as a catastrophic rise event of 13.5 m in magnitude starting at 14.2 ka (*8*), and as a rapid sea-level rise of 24 m in 500 years (14.2 to 13.7 U/Th ka) [less than 1.0 ^{14}C ka around 12 ^{14}C ka corresponding to 14.5 to 13.6 ka (*1, 2*)]. Our record thus provides additional evidence for the existence and importance of MWP 1A and shows that sea level dramatically rose by as much as 16 m within 300 years. The sea-level curve shows a continuous sea-level rise before and after one accelerated short-lasting period due to a major melting event in the polar regions.

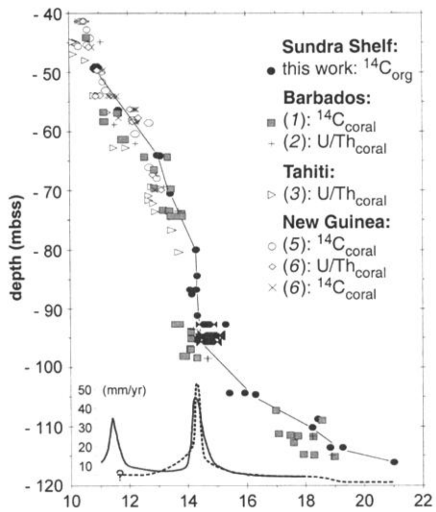

Fig. 2. Compilation of sea-level data in comparison. Solid line, Sunda Shelf sea-level curve; using *Acropora* palmata (*1, 2*), and using different coral (sub)species (*3, 5, 6*). Note significant distance between ^{14}C data points from Barbados and the Sunda Shelf, both based on ^{14}C ages calibrated using INTCAL98/CALIB4. Dotted line below, rate of glacial meltwater discharge calculated from Sunda curve; solid gray line, rate of discharge from Barbados using U/Th ages. Discrepancies between both are within 1σ. mbss = meters below sea surface.

References and Notes

1. R. G. Fairbanks, *Nature* **342**, 637 (1989); *Paleoceanography* **5**, 937 (1990).
2. E. Bard, B. Hamelin, R. G. Fairbanks, A. Zindler, *Nature* **345**, 405 (1990).
3. E. Bard *et al.*, *Nature* **382**, 241 (1996).
4. L. Montaggioni *et al.*, *Geology* **25**, 555 (1997).
5. J. Chappell and H.A. Polach, *Nature* **349**, 147 (1991).
6. R. L. Edwards *et al.*, *Science* **260**, 962 (1993).
7. Ages in calendar years before present (1950 A.D.) are expressed in thousands of years (ka). ^{14}C ages have been calibrated to calendar years by using the INTCAL98 calibration set and the calibration program CALIB 4.0 [M. Stuiver *et al.*, *Radiocarbon* **40**, 1041 (1998); E. Bard, M. Arnold, B. Hamelin, N. Tisnerat-Laborde, G. Cabioch, *Radiocarbon* **40**, 1085 (1998)], which is distinctly different from the earlier version.
8. P. Blanchon and J. Shaw, *Geology* **23**, 4 (1995).
9. P. T. Harris, *Sediment. Geol.* **125**, 235 (1999).
10. H. D. Tjia and K. K. Liew, in *Tectonic Evolution of Southeast Asia*, R. Hall and D. Blundell, Eds. (Geology Society Special Publication 106, Geological Society, London, 1996), p. 291; T. O. Sinandjuntak and A. J. Barber, in *Tectonic Evolution of Southeast Asia*, R. Hall and D. Blundell Eds. (Geology Society Special Publication 106, Geological Society, London, 1996), p. 185.
11. Q. Zhao, Q. Li, P. Wang, Eds. *WESTPAC Paleoceanographic Maps*, (Unesco/IOC Publication, Marine Geology Laboratory, Tongji University, Shanghai, 1995).
12. H. D. Tjia, *Z. Geomorph. N.F.* **24**, 405 (1980).
13. K. Stattegger *et al.*, *Ber. Rep. Geol. Paläontol. Inst. Univ. Kiel* **86**, 211 (1997). The inner shelf is dominated by low sedimentation rates and erosion after the LGM, the middle shelf by highly differentiated coastal deposits belonging to a transgressive system, and the shelf margin by large depositional hiatuses. A major fault (Lupar line) running from western Borneo, easterly Natuna Island, to the continental slope off Vietnam seems to have been inactive during the last tens of thousands of years (*10*). Additionally, a system of small-scale faults observed in our seismic survey results in gravitational mass movement near the shelf break.
14. T. Hanebuth and K. Stattegger, *Mar. Geol.*, in press; T. Hanebuth, unpublished data; A. Richter, thesis, University of Kiel, Kiel, Germany (1998); A. Schimanski, thesis, University of Kiel, Kiel, Germany (1999).
15. P. A. Pirazzoli, *World Atlas of Holocene Sea-Level Changes* (Elsevier, Amsterdam, 1991), p. 117; *Singapore Tide Gauge* (Horsburgh Lighthouse).
16. AMS ^{14}C ages were measured with a 3-MV high-voltage engineering Europa Tandetron 4130 AMS system to a precision (counting statistics and machine statistics) of 0.3% for modern samples. This resulted in typical ^{14}C age uncertainties (1σ) of 50 to 80 years. M.-J. Nadeau *et al.*, *Nucl. Instrum. Methods B* **123**, 22 (1997); M.-J. Nadeau *et al.*, *Radiocarbon* **40**(1), 239 (1998).
17. P. B. Tomlinson, *The Botany of Mangroves* (Cambridge Univ. Press, Cambridge, 1986). The mangrove, as a highly sensitive sea-level indicator, belongs to the tidal range between mean sea level and mean high water datum. The detailed biozonation of mangrove habitat is negligible in this case because of the microtidal character in this area.
18. The ash content of carefully cleaned organic material from the tidal flat environment indicates very rapid burial of litter after death in the mangrove swamp without any significant decay [see R. A. Gastaldo, G. P. Allen, A. Y. Huc, *Geol. Soc. Am. Spec. Pap.* **286**, 107 (1993)]. Measurement of $\delta^{13}C_{org}$ and the age difference of humic acids to leach residues adds further information to help recognize fresh material.
19. Supplementary figure is available at www.sciencemag.org/feature/data/1046133.shl.
20. Supplementary table is available at www.sciencemag.org/feature/data/1046133.shl.
21. A number of primary and secondary natural effects on control of true ages have been considered—for example, tidal range, material mixing, changes in ^{14}C production, and subsidence and uplift. There is no evidence for compaction of these young sediments. Bioturbation is also negligible because of very high sedimentation rates locally. If we take into account that the equatorial ocean siphoning [J. X. Mitrovica and W. R. Peltier, *J. Geophys. Res.* **96**(B12), 20053 (1991)] secondarily decreased the water depth by several meters, our value corresponds well with the generally estimated depth of about −120 m during LGM and therefore does not indicate a significant effect of hydroisostasy [K. Fleming *et al.*, *Earth Planet. Sci. Lett.* **163**, 327 (1998)]. Another aspect that is probably important is the effect of gravity field and centrifugal force on the global distribution of newly generated water masses in a scale of meters, as mentioned by W. R. Peltier [*Science* **265**, 195 (1994)].
22. If we assume that there is a minor chance of sampling the first coral individuals that started to colonize the substratum and that coral settling started 200 to 300 years after inundation (*4*), we find an almost perfect match with the record of terrestrial organic material from the Sunda Shelf, which provides direct age control within the time interval of missing coral ages. If we further consider a significant rise in atmospheric CO_2 caused by adding large amounts of CO_2, probably from the ocean (i.e., ^{14}C depleted), we expect a drop in atmospheric ^{14}C. This we see as a plateau. If the corals are in direct exchange with the atmosphere, then they should not have the 400-year reservoir age subtracted and end up with an age similar to our organics. If they do have a 400-year reservoir age, then the drop in atmospheric ^{14}C will reach the corals with (some) delay, thus reducing their apparent reservoir age during the ^{14}C plateau. This works together with the coral startup time and sampling to explain the observed discrepancies.
23. M. Stuiver, P. M. Grootes, T. F. Braziunas, *Q. Res.* **44**, 341 (1995); P. M. Grootes, M. Stuiver, J. W. C. White, S. Johnsen, J. Jouzel, *Nature* **366**, 552 (1993).
24. Project 03G01115A was supported by the German Ministry of Education and Research. T.H. acknowledges a graduate school stipend funded by the Deutsche Forschungsgemeinschaft. We thank the team from the Leibniz Laboratory in Kiel for support and assistance. We gratefully acknowledge the positive comments by C. D. Woodroffe and two anonymous reviewers.

11 October 1999; accepted 7 January 2000